Energy Efficiency in IoT Networks: Integration of Reconfigurable Antennas in Ultra Low-Power Radio Platforms Based on System-on-Chip

# Energy efficiency in IoT networks: Integration of Reconfigurable Antennas in Ultra Low-Power Radio Platforms Based on System-on-Chip

Simone Ciccia*, Giorgio Giordanengo*, Giuseppe Vecchi†, *Fellow, IEEE*
* Advanced Computing and Electromagnetics, LINKS Foundation, 10138 Torino, ITALY
†Department of Electronics and Telecommunications, Politecnico di Torino, 10129 Torino, ITALY

***Abstract*—The current state of the art of Internet of Things witnesses the development of low-cost and smart-connected wireless sensor networks placed at the edge of clouds, enabling new services over the internet. In these interconnected smart sensors, energy consumption is an important issue. This work deals with decreasing energy consumption in wireless sensor network nodes by means of antennas with reconfigurability at radiofrequency. Our research has yielded two important novelties. First, the reconfiguration is accomplished with a platform comprised of a commercial ultra low-power micro-controller and system-on-chip radio. Second, we consider explicitly the energy overhead involved in the antenna configuration process and its impact on the global energy efficiency of the system. We discuss two complementary ways of reducing the energy consumption; one by lowering the amount of transmitted power, the other by increasing the transmission rate. We employ an antenna array with a steerable beam, controlled by an algorithm embedded in the firmware of the ultra low-power platform. This is designed for line-of-sight conditions, and the beam steering maximizes the received power. Our results show that with a common IEEE 802.11 b/g system-on-chip module and an antenna gain of 12$dB$, a net power saving factor of 28% can be obtained by reducing the transmitted power, at unchanged data rate; additionally, by keeping the transmit power constant, but increasing the data rate, an energy saving from 18% to 96% can be achieved, depending on the link distance and achievable data rate. Our experiments have confirmed both routes of energy saving.**

***Index Terms*—Energy efficiency, Reconfigurable antennas, Ultra low-power communications, Wireless Sensor Networks, Internet of Things.**

## I. Introduction

WIRELESS Sensor Networks (WSN(s)) are widely employed in Internet of Things (IoT) for sensing and transferring information [1]–[3]. In this scenario, IoT is seen as a network of WSN(s), with the purpose of aggregating data from all sensors (i.e. egde gateway) and send to the edge server [4], [5]. There are several IoT applications that rely on such network topology, as for example Industry4.0, environmental observation, disaster monitoring, smart city, traffic control and monitoring, and all demanding for reliable throughput which is often questionable (i.e. real-time constraints) [6]–[9].

Manuscript received November X, 2018; revised Month DD, 201Y. Corresponding author: S. Ciccia (email: simone.ciccia@linksfoundation.com). 

Energy efficiency of IoT WSN(s) is a critical issue. The main reason for this concern is the fact that the nodes in the WSN(s) sub-system are mostly supplied by renewable sources and/or small batteries [10]–[14].

Several techniques to improve the lifetime of a node have been presented in the literature, especially to lower the consumption of the radio part [15]–[19]. In the following, we attempt a nonexhaustive review of the proposed approach. One approach is to modify the communication protocol [15]–[17]. For example, in [15] the sensor node is allowed to adjusts the transmitted power based on received parameters; i.e. the link quality is adaptively analysed to select an appropriate transmitted power level, which allows reducing the consumption of a node by saving the unnecessary transmitted power. In [18], the transmit power level is assigned to each sensor node based on the network geometry (e.g. link distance). Another option is scheduling transmissions [19]. This consists in a sleep/awake mechanism which activates the radio only when a data transfer is required. Where applicable (e.g. in environmental and traffic monitoring systems), this obviously allows an energy saving (as long as the sleep/awake mechanism does not require a significant energy).

The use of a directive antenna allows a higher received power with all other factors unchanged, since the received signal is proportional to the transmitted power and the product of the gains of Receiver (RX) and Transmitter (TX) antennas. Therefore, this can provide an energy gain either alone, or in synergy with any other energy saving approach [17]–[20]. It is well known that higher antenna gain can only be achieved by a non-omnidirectional antenna, thus a steerable beam that can be adapted to different link directions is required, as an example in [21]–[23]. Since the beam direction needs to be changed either dynamically, or at least automatically in the initial deployment, the necessary antenna systems are termed ”reconfigurable”.

### A. Reconfigurable antennas for energy saving: state of the art

Despite the good prospects of reconfigurable antennas, this energy saving option is not yet fully exploited in WSN(s) for several reasons. The main reason is attributed to the difficulty of effectively integrating these antenna systems in low-power architectures. In the following, we review the approaches in the literature; we will then address our approach and its innovation with respect to the state of the art in next Section.

The work in [24] is a good illustration of antenna integration. In this study, the authors attempt to integrate a switched beam antenna into a radio based on System on Chip (SoC). The main weakness with this approach is that it relies on a Linux Operative System (OS) which entails a consistent power consumption overhead to run.

A wake-up method along with reconfigurable antennas is presented in [25]. This experiment illustrates the use of two reconfigurable antennas, one for continuously monitoring the position of the base station and one to transmit data in the right direction when required. Unfortunately, this specific sensor has the receive circuitry constrained to be always on, with associated power consumption.

Another interesting work discusses how controllable directive antennas achieve transmission power saving as a result of minimizing the collision rate at the gateway side [26]. In that work, a switchable beam antenna and the related consumption for its configuration were analyzed. However, the impact of energy required for the antenna configuration phase has not been considered in the *global* energy efficiency of the system. This initial energy overhead is negligible in a static scenario with a single configuration phase; in a scenario where the positions of nodes can change dynamically, this overhead has to be considered with respect to the (average) time between changes. This aspect will be considered in this work.

A number of other works have addressed the issue of reconfigurable antennas for energy saving in WSN(s) [20], [22], [25], [27]–[30] and in a specific IoT context [8], [9]. Some of the accounts are of purely simulative nature [8], [9], [20], [22], [28]–[30]; those addressing actual antenna reconfiguration considered this either in stand-alone [27] or in association to a system [25], [26] only for short-range and low-rate wireless standards, i.e. Low-Power Wide-Area Networks (LPWAN). LPWAN is less considered for real-time sensors since it often provides unreliable bandwidth [31].

In contrast with this, our work addresses the integration of the reconfigurable antenna in the IEEE 802.11 b/g ST SoC-radio. This communication standard has been selected for the following reasons:

1) it provides enough throughput for the selected application;
2) it has a robust data encryption which provides protection against cyber attacks, privacy and data integrity.

All of them are key factors to properly design an IoT WSN(s) [32], [33].

This choice is neither restrictive nor limited to other actuation forms that are widely used in both IoT-sensing and edge layer [34]. It is important to mention that the proposed solution does not alter the communication protocol. This enables such approach to any other radio (e.g. 802.11 family-standards, LoRaWAN, Bluetooth Low Energy).

A common feature of all these works is the neglect of the consumption dedicated to the antenna configurations in the total energy budget. This issue will be addressed in the present work.

### B. Proposed approach

Figure 1 sketches the employment of reconfigurable directive antennas in the IoT scenario described in the introduction. A point of interest is that different layers have different requirements. Indeed, the main issue of WSN(s) is energy efficiency, while the edge layer has real-time constraints. This work focuses on the energy efficiency in WSN(s), and highlights the actual advantages that can be exploited in the edge layer. The first goal of this work is the integration of

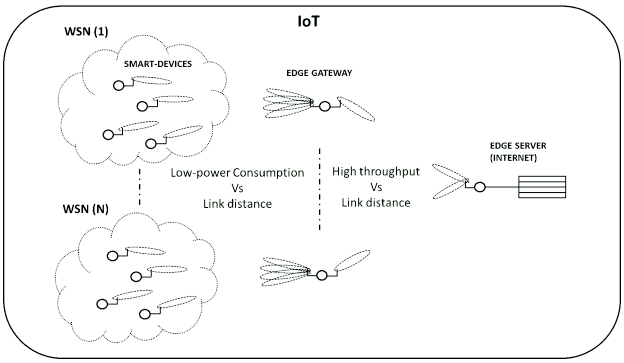


Fig. 1. IoT scenario with reconfigurable directive antennas alluded in the introduction.

a reconfigurable antenna in an Ultra Low-Power (ULP) SoC-based system. The ULP performance comes from the ULP micro-controller that manages the SoC radio module; antenna reconfiguration is effected by a firmware algorithm running on the ULP micro-controller. We demonstrate the proposed approach on a system composed by low-cost commercial devices, a ULP micro-controller and a SoC radio. The second goal is to test and validates the advantages of the proposed approach in the field.

Antenna (re)configuration does produce the described advantages, but this comes at an energy cost that has never been considered so far [20], [22], [24]–[26], [28]–[30]. Indeed, any search and any processing implies an on-time spent without transmitting useful data, and the associated overall energy cost; this configuration overhead needs to be accounted for to achieve a true energy gain. To the best of the authors' knowledge, an analysis on the energy efficiency provided by reconfigurable antennas still lacks in literature and will be addressed in this paper for the first time.

In contrast to the approach presented in [24], [27], our system relies on a small firmware which avoids the (large) power consumption related to the OS. We exploited a common micro-controller (STM32 Nucleo) which consumes a power of a hundred $mW$ as opposed to the $W$ required by a low-power board to run an OS.

To overcome the discussed limitations of the approach in [25], we propose an energy efficient link where the edge gateway is in charge of continuously scanning the space and finding which sensor node requests to transmit. Sensor nodes are activated by their own radio awakening system and transmit only when the collected data need to be transferred (with the adopted policy). At this side, the antenna configuration phase is performed at each wake-up (or at least once if the node

location is static). Since the edge gateway has less stringent energy requirements than the sensor nodes, this approach is advantageous. This notwithstanding, the number of antenna search (i.e. the "configuration process") must be carefully considered at sensor side, since this number influences the overall lifetime of the node. This will be discussed later.

Another advantage of the proposed solution is that we consider a network architecture that does not need to be of a star type (i.e. single hop) [26]. Indeed, our system can operates in any network configuration, both single-hop and multi-hop (e.g. a WSN(s) node can work as a bridge). Furthermore, we have not altered the MAC protocol.

An important aspect of this work with respect to [26] and the current literature is the consideration of a dynamic scenario where true re-configuration may be necessary due to changes in the WSN(s) geometry.

We also observe that a WSN(s) system equipped with such a reconfigurable directive antenna has two complementary advantages with respect to the standard (omnidirectional) antenna:

- At the same link distance, one can achieve the same received power with a lower transmitted power; hence, one can have the same data rate as with a standard system, with unchanged data link performance, but with a lower transmitted power. In this case, there is a power saving, since power consumption of the wireless device is proportional to the transmitted power. Then, a given quantity of information is transferred with a lower energy because of the lower transmitted power. This is the traditional motivation of higher antenna gains.
- Alternatively, with the same transmitted power, there is a higher received power, which allows to transmit data at higher rates. This implies that a given quantity of information can be transferred in a shorter time (i.e. with a smaller energy). This alternative strategy to energy saving has rarely considered in the literature.

The two advantages can be combined, and this approach will be addressed in the following, as an effective means to lower the energy-per-bit cost.

For the edge gateway, throughput maximization is preferred since it has to transfer large quantities of data coming from all sensors. Reconfigurable directive antennas play a crucial role in this scenario. As a matter of fact, directional links provide robustness against interference and boost channel capacity. Indeed, reliable data transfer is achieved with high gain directive antennas and low levels of transmitted power (i.e. low signal distortion), as well assessed in Fifth Generation (5G) and Millimeter Waves (mmWave) communication technologies [35].

The key factor influencing the reconfigurable antenna design is determined by the link distance to cover, and hence the necessary gain. For long distance connections, phased array antennas are able to provide a better (finer) beam alignment; on the other hand, their gain decreases for increasing scan angle, thus limiting the scan range. Conversely, switchable beam antennas can in principle provide an overall scan range of 360 degrees, but with coarser alignment and (for equal size) limited maximum gain (with equal computation complexity and scan time) [36]–[39]. Since our tests have been applied to the traffic monitoring use case, with a required coverage of $1km$, we selected a steerable beam antenna array to prove the concept. We stress however that our method and conclusions apply to the switchable beams as well.

### C. Structure of the paper

The rest of the paper is organized as follows. Section II presents the employed method in order to analyze the performance of the proposed system with respect to the baseline depicted in Figure 2. Section. III introduces the hardware and software components involved in the realization of the proposed system, with special attention to the ULP SoC-based radio platform, the designed antenna and the developed firmware. Section. IV details the consumption profile of the system in possible scenarios. Finally, Section. V reports the field test and then some conclusions are drawn.

## II. Background and Analysis Method

### A. Link budget

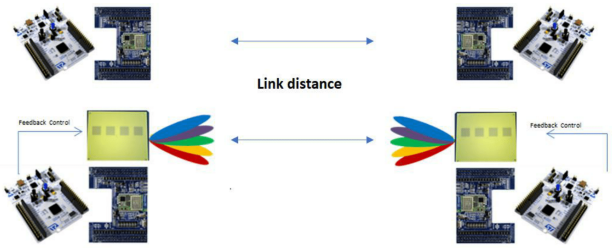


Fig. 2. State-of-the-Art link (top) vs reconfigurable antennas link (bottom).

The analyzed scenario is depicted in Figure 2 and illustrates the State-of-the-Art Wireless (SAW) system (top) and the proposed Reconfigurable Antenna Wireless (RAW) system (bottom). The SAW system is composed by the SoC-based radio sold with an integrated antenna that has an omnidirectional coverage [40], while the proposed RAW system exploits the SoC module sold with the U.FL connector and integrates the proposed reconfigurable antenna which provides a directive beam towards the intended direction.

The first quantity of interest is the received power that was evaluated with the Friis formula [41]. This is described by:

$$P_{rx} = P_{tx} + G_{tx} + G_{rx} - L_{att} \; [dBm] \tag{1}$$

where $P_{rx}$ is the received power in $dBm$ that we will consider as Receive Signal Strength Indication (RSSI) since in Line of Sight (LoS), $P_{tx}$ is the transmit power in $dBm$, $G_{tx}$ and $G_{rx}$ are the transmit and receive antenna gains respectively and $L_{att}$ is the overall attenuation defined in the following way:

$$L_{att} = L_{path} + L_{add} \; [dB] \tag{2}$$

where $L_{add}$ is an additional loss that accounts for cable losses at the transmitter and receiver side respectively, while $L_{path}$ is the pathloss which is in turn described as:

$$L_{path} = 20 \log_{10}(\frac{4\pi d f_{max}}{c}) \; [dB] \tag{3}$$

where $d$ is the link distance, $c$ is speed of light and $f_{max}$ is the maximum operating frequency.

### B. Power saving

A significant point of the link budget comparison analysis is that the RAW link can lower the transmit power and/or increase the data rate with respect the SAW link; the related saving in transmit power is obtained by equating the received power, which yields:

$$P_{save} = P_{tx,SAW} - P_{tx,RAW} = \\ = (G_{tx,RAW} - G_{tx,SAW}) + (G_{rx,RAW} - G_{rx,SAW}) \; [dB] \tag{4}$$

The power saving enabled by the antenna gain difference $P_{save}$ is effected via control of the Programmable Gain Amplifier (PGA), and it could be limited by the minimum PGA gain that can be set in the device. This will be further discussed in Section IV-B.

### C. Energy saving for equal data rate

Lowering the transmit power is one of the ways to save energy. This is achieved with beam alignment. Thus, a *configuration phase* is required. We will now investigate the impact of energy consumption for the antenna configuration phase on the overall operation. We underline that the RAW system always begins in energy debit with respect to the SAW system. Thus, we examine how long the RAW system takes to reach the energy breakeven point, i.e. the time at which the RAW system power saving has equated the energy spent in the configuration phase. If the scenario does not change, after that time the RAW system always saves energy. This energy breakeven is an important parameter to judge the effective advantage of the RAW approach with respect to the intended system scenarios: an energy saving happens if the system scenario changes (e.g. relocation of nodes) are slower than the time scale set by the breakeven time.

The energy consumption of the non-reconfigurable (SAW) system is given by:

$$E_{SAW}(\Delta t) = \int_{t_0}^{t_0+\Delta t} P_{a,SAW} \; dt \; [J] \tag{5}$$

where $t_0$ is an initial time, $P_{a,SAW}$ is the power absorbed by the SAW system during data transfer, and $\Delta t$ is the considered data transfer duration. To transmit the same amount of data, the reconfigurable system RAW set the same data rate, and thus the same transmit time $\Delta t$, but requiring a lower power $P_{a,RAW}$; hence the associated energy cost is:

$$E_{RAW}(\Delta t) = E_{scan} + \int_{t_0}^{t_0+\Delta t} P_{a,RAW} \; dt \; [J] \tag{6}$$

where $E_{scan}$ is the energy required for the antenna configuration phase. In this phase, for each searched direction, it has to point the beam in the given direction, transmit a beacon frame and acquire the result to form a decision on the searched direction; this per-direction cost has to be multiplied by the number of necessary search directions $N_p$. The beam pointing phase will be labeled with "BP"; this phase is used to configure the Digital to Analog Converters (DAC) needed to drive the analog phase shifters. The acquisition phase corresponds to the time $t_{ACQ}$ required to perform a Service Set IDentifier (SSID)/RSSI search. Neglecting the consumption dedicated to transmit the short beacon, in both phases the power absorption is mainly due to the reception state and the overall energy cost can be written as:

$$E_{scan} = N_p \left( \int_0^{t_{BP}+t_{ACQ}} P_{rx} \; dt \right) \; [J] \tag{7}$$

where $P_{rx}$ is the power absorbed during the beam pointing phase and the SSID/RSSI search. On the other hand, the initial time at which useful data transmission starts is now $t_0 = t_{BP} + t_{ACQ}$.

The breakeven achieves after a time $\Delta t = t_{be}$ for which $E_{SAW}(t_{be}) = E_{RAW}(t_{be})$. The involved powers are typically constant during the related time phases, and the integrals simplify to a product, thus giving:

$$t_{be} = \frac{E_{scan}}{P_{a,SAW} - P_{a,RAW}} \; [s] \tag{8}$$

The term $t_{be}$ gives an estimation of how long the RAW system needs to wait in order to perform another antenna configuration without exceeding the consumption of the SAW.

### D. Energy saving for variable data rate

A second way to save energy is through increasing the data rate. Indeed, as long as the power absorbed by the radio module does not depend on data rate, the energy required to transmit a frame is reduced if the transmit time is lowered. This happens by increasing the data rate. This invariance of absorbed power with data rate will be described in the appropriate Section IV.

In this case, the energy consumption is expressed as:

$$E_{SAW}(N_f, R) = N_f \int_{t_0}^{t_0+t_f(R_{SAW})} P_{a,SAW} \; dt \; [J] \tag{9}$$

$$E_{RAW}(N_f, R) = E_{scan} + N_f \int_{t_0}^{t_0+t_f(R_{RAW})} P_{a,RAW} \; dt \; [J] \tag{10}$$

where $t_f(R)$ represents the frame duration, which is a function of the achieved data rate. The latter is a function of the receiver sensitivity which defines the required receive power level in order to use a specific modulation (this characteristics is usually declared in the receiver datasheet [42]).

The energy breakeven can be found equating (10) with (9):

$$N_f^{be}(R) = \frac{E_{scan}}{(P_{a,SAW} \; t_f(R_{SAW})) - (P_{a,RAW} \; t_f(R_{RAW}))} \; [s] \tag{11}$$

where $N_f^{be}(R)$ is the number of transmitted frames that achieves breakeven, while $t_f(R_{RAW})$ and $t_f(R_{SAW})$ are the frame duration related to the data rate employed by the RAW and the SAW system respectively. Equation (11) states that the quantity of information (number of frames) that has to be transmitted before another antenna configuration can be performed to breakeven with configuration energy cost.

## III. Implementation and Description of the Proposed System

### A. STM32 Nucleo

The STM32 Nucleo platform, depicted in Figure 3a, is a ULP Advanced Reduced instruction set computing Machine (ARM)-based micro-controller programmable on-the-fly by means of a firmware [43]. This solution provides fast prototyping and flexibility since:

- has a comprehensive software library that can be easily included in a standard ANSI C program;
- provides the standard General Purpose Input/Output (GPIO)s to interface external radio modules, as the IEEE 802.11 b/g, LoRaWAN and other SoC radios;
- offers a pinout that can be configured as DACs, Pulse Width Modulator (PWM)s and switches. They can be used to control beamformers.

### B. SoC-based radio

The radio module, depicted in Figure 3b, is based on a low-power IEEE 802.11 b/g SoC which expands the STM32 Nucleo boards with wireless capability [42]. This wireless module integrates a PGA which controls the transmit power. The module allows to configure the network topology as access point, ad-hoc and infrastructure mode.

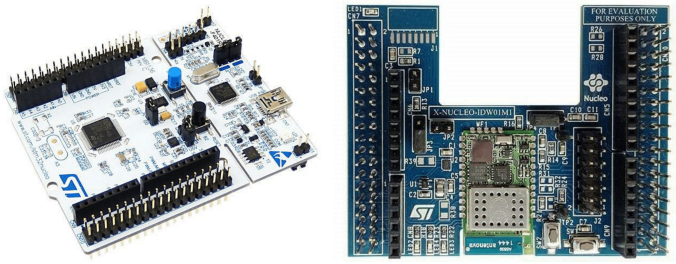

(a) (b)

Fig. 3. Main components of the ULP radio platform (STM32 Nucleo Platform and SoC-based radio): ULP micro-controller (a) and Low-power IEEE 802.11 b/g SoC-based (b).

### C. Reconfigurable antenna

The antenna realized for the test is composed by two parts, i.e. the radiating elements, depicted in Figure 5a and the Beam Forming Network (BFN), Figure 5b. Together, they form a conventional phased array.

The radiating element is an aperture coupled microstrip patch, whose structure is reported in Figure 4a and the details in Figure 4b [44]. The Patch is printed between two substrates, IS400 and Rohacell-HF31 ($e_r$ = 4.46 and 1.05, $h$ = 1.55 and 4 $mm$ respectively) [45], [46]. The proposed structure has the following advantages:

1) the aperture coupled feed (i.e. slot) avoids reflections (losses) due to otherwise soldered probe feed;
2) the wider thickness of the Rohacell-HF31 substrate (between ground and radiating elements) helps to increase the patch antenna bandwidth;

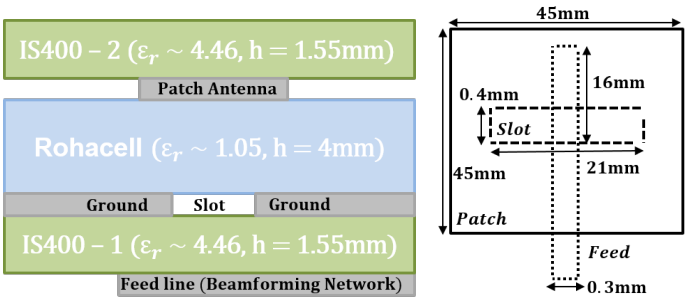


(a) (b)

Fig. 4. Reconfigurable antenna: Substrate-stacked structure of a radiating element (a) and main quotes (b).

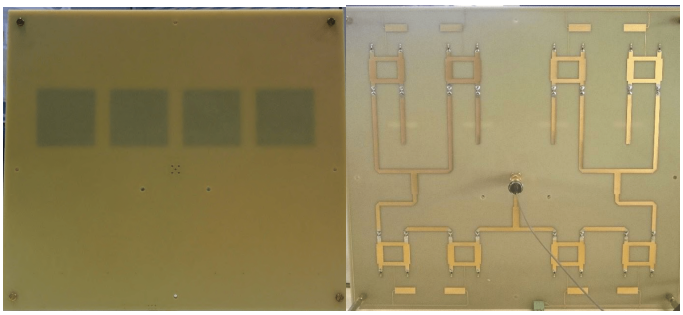

(a) (b)

Fig. 5. Reconfigurable antenna: Radiating elements (a) and Beam Forming Network (b).

3) the upper IS400 layer keeps the radiating elements safe from deterioration and external contacts, since the patch antennas face the internal part of the structure.

Inter-elements distance is computed by considering the grating lobe limit formula:

$$d \leqslant \frac{1 - 1/N}{1 + \mid cos(\alpha_{max}) \mid} \lambda_0 \qquad (12)$$

where the term $N$ represents number of radiating elements, $\alpha_{max}$ is the maximum scan angle while $\lambda_0$ is the free space wavelength [47]. Equation (12) ensures that the grating lobe does not enter in the visible range of the radiation pattern when the main beam is steered at the maximum scan angle $\alpha_{max}$. With a 4-element array and a desired scan angle of 45°, (12) gives an inter-elements distance of 65 $mm$. This configuration form a directive beam in the scan plane with a maximum gain of 12$dB$ and approximately 30° of Half Power Beam Width (HPBW), while a wider beam in the vertical plane with a HPBW of about 60°. Figure 6 shows the measured radiation pattern for horizontal and vertical planes.

The BFN, which is formed by one input and four outputs, is in charge to perform the beam steering. The latter is achieved by assigning a phase excitation to each radiating element (while keeping a uniform amplitude distribution). Phase excitations are generated by continuously varying the DC voltage of several quadrature couplers [48]. When the coupler is loaded by two varactors, then a quasi-linear relation between the applied voltage and the output phase is obtained.

In this way, each branch of the BFN is controlled with a phase excitation. When no voltage (or the same voltage) is applied to the BFN branches, the array is pointing broadside, since the phase difference among all output ports is zero. When different voltages are applied to the BFN branches, the main beam is moving in the scan plane. Varactor details can be found in [49]. The realized array performs a scan in the range ±45°.

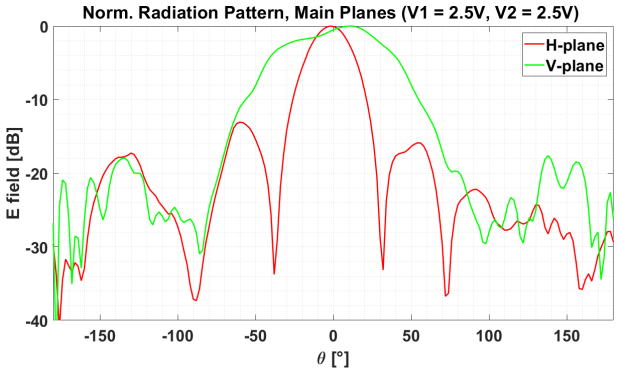


Fig. 6. Reconfigurable antenna: Measured radiation pattern (horizontal and vertical plane).

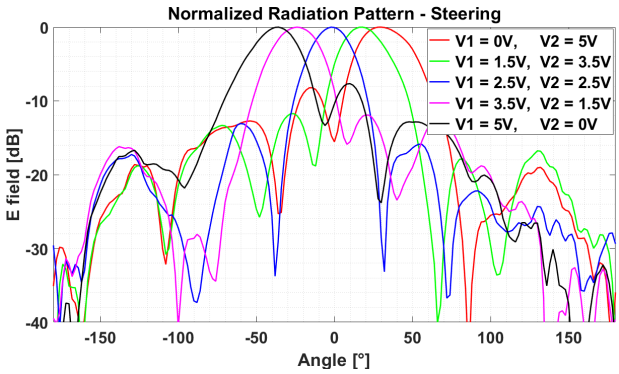


Fig. 7. Reconfigurable antenna: Measured radiation pattern (steering capability in the scan plane).

Some example of measured radiation patterns are depicted and in Figure 7.

The entire structure has the dimensions of $230mmx260mmx7mm$ and the antenna operates in the Industrial, Scientific and Medical (ISM) frequency band $2.40 - 2.48GHz$ and it comes with an SMA to U.FL connector to directly interface the radio module described in Section III-B. The measured reflection coefficients for the antenna prototypes are reported in Figure 8, which shows a good matching (return loss lower than -15$dB$) in the overall bandwidth.

### D. Developed firmware

The advanced wireless communication capabilities are managed by a firmware running on the ULP STM32 Nucleo board described in Section. IV. For the intended application, the STM32 Nucleo firmware is configured with the minimum number of peripherals needed:

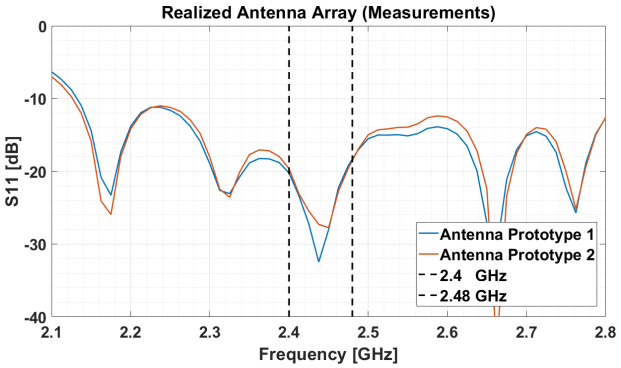


Fig. 8. Reconfigurable antenna - Measured reflection coefficient (S11).

- on-board DAC to configure the desired direction of radiation (i.e. antenna beam steering);
- an intrinsic Universal Asynchronous Receiver-Transmitter (UART) interface to transfer data between the STM32 Nucleo micro-controller and the SoC Wi-Fi radio;
- Serial Peripheral Interface (SPI) to transmits and receive information with other modules (e.g. a camera board).

The optimization algorithm provides the right voltage value to steer the antenna main beam in the best direction (i.e. through DAC); this is integrated in the firmware of the STM32 Nucleo.

The working principle of the energy efficient wireless link is the following.

1) The edge gateway continuously steers the main beam to find an awoken sensor node. The latter is off for most of the time unless some data need to be transferred.
2) As soon as the radio platform of the sensor is powered, then the base station directs its beam toward it. The STM32 micro-controller takes approximately 10 seconds to initialize itself (independently from the employed antenna).
3) This antenna configuration process is then repeated by the sensor.
4) When the beams are aligned, then the transmission starts and the link can profit of the energy savings discussed in Section II.

## IV. Power Consumption and Performance

### A. Wireless radio module: power consumption analysis

The power consumption measurements of both SAW and RAW have been performed to confirm the improvements. The measurement setup is summarized in Figure 9. A small sense resistance ($2.8\Omega$) is placed in series to the positive $5V$ cable which supply the full system. A high-impedance oscilloscope ($1M\Omega$), has been exploited as probe in parallel to the sense resistance, to measure the voltage drop. Since this voltage drop is proportional to the absorbed current, the latter is estimated by simply dividing the voltage drop by the sense resistance. Each prototype has been measured during data transmission by changing the transmit power from 0 to 18 $dBm$ and the related consumption reported in Table I. From the measured data, it can be asserted that the consumption of developed RAW system is almost the same. To be more

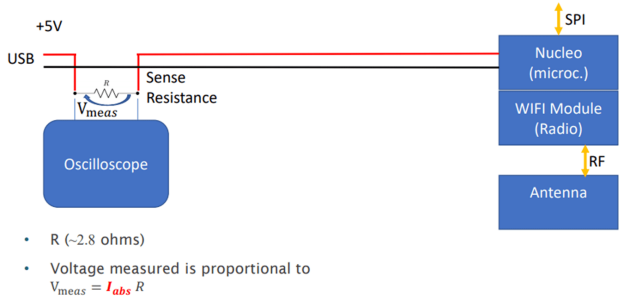


Fig. 9. Setup to measure the power consumption of the SAW and RAW platforms.

TABLE I
OVERALL SOC-BASED RADIO AND STM32 NUCLEO STATES.

| Radio State | TX Power $P_{tx}[dBm]$ | SAW Abs. Current $I_a[mA]$ | RAW Abs. Current $I_a[mA]$ |
|---|---|---|---|
| TX | 0 | 164.3 | 166.3 |
| TX | 3 | 167.0 | 169.0 |
| TX | 6 | 171.4 | 173.4 |
| TX | 9 | 186.0 | 188.0 |
| TX | 12 | 193.0 | 195.0 |
| TX | 15 | 214.3 | 216.3 |
| TX | 18 | 228.6 | 230.6 |
| RX | - | 85.7 | 87.7 |

precise, the power consumption of the steerable antenna has been measured separately, and a value of $400\mu A$ has been found. This additional current absorption is largely due to a low-power operational amplifier used to drive the varactors (i.e. MCP6002) and in a lesser extent due to the 16 varactors [50]. We remark that this energy consumption, inherent in the reconfiguration function, is fully accounted for in our energy budget in Sections IV-B, IV-C and measured data in Table I. From this number we can said that the reconfigurable antenna does not increase the overall power consumption of the radio. We did not reported the sleep consumption of the system since in our configuration the radio is off (i.e. not supplied) when no data need to be transmitted. The frame duration, which depends on the employed data rate (i.e. modulation), was also investigated. This estimation, reported in Table II, has been performed considering $1000B$ of information per frame. The latter consists of a header composed by $24B$ always transmitted at $1Mbps$, thus providing a fixed timing of $192\mu s$. A second header is added to the highest data rate only (i.e. the IEEE 802.11g) and consist of $4B$ transmitted at the selected rate; however its impact on the overall frame is not so relevant. The rest of the frame duration is given by the quantity of information bytes divided by the selected rate. Table II also reports the required sensitivity which defines the minimum RSSI level required to employ a specific data rate. This information can be found in datasheet [42].

### B. Overall energy saving for equal data rate

The power saving estimation, in (4), is readily done with the system parameters. In our case the integrated antenna of the SAW has a maximum gain $G_{tx,SAW} = G_{rx,SAW} \approx 2dB$; the RAW system has a maximum gain of $G_{tx,RAW} = G_{rx,RAW} = 12dB$ in the broadside setup, with a gain decrease of $2dB$ at the maximum scan direction of 45°. A power saving $P_{save}$ ranging from $20dB$ to $16dB$, depending on whether the link is in the broadside direction of both antennas (best case), or at maximum scanning angle of both (worst case) is achieved. With the available hardware, the dynamic of the programmable gain amplifier is limited to $18dB$. As a consequence, the best case of the power save is limited to this range. These expected power savings have indeed verified by measuring current absorption, resulting in a net power saving from 26.0% (worst alignment) to 27.3% (gain saturation), with respect to the maximum transmit power consumption of the SAW $228.6mA$.

TABLE II
FRAME DURATION FOR DIFFERENT ACHIEVABLE DATA RATES DEFINED BY THE STANDARD IEEE 802.11 B/G.

| IEEE802.11b/g Standard | Rate $R[Mbps]$ | Sensitivity $RSSI[dBm]$ | Frame time $t_f[\mu s]$ |
|---|---|---|---|
| 802.11b | 1.0 | -96 | 8192 |
| 802.11b | 2.0 | -93 | 4192 |
| 802.11b | 5.5 | -91 | 1646 |
| 802.11b | 9.0 | -89 | 1080 |
| 802.11b | 11.0 | -87 | 919 |
| 802.11g | 18.0 | -86 | 638 |
| 802.11g | 36.0 | -80 | 415 |
| 802.11g | 54.0 | -74 | 340 |

The energy dedicated to the antenna configuration phase has to be accounted for to estimate an accurate energy saving. In our case, $900ms$ are necessary to move the beam (i.e. set DAC ) and perform the SSID/RSSI evaluation. The overall consumption of the antenna configuration phase depends on the required RSSI accuracy in the scan plane. In other words, the proposed antenna has a HPBW of 30°, thus an appreciable change of $3dB$ in RSSI is sensed by steering the main beam with steps of 15°. As a result, only 7 points (i.e. −45°, −30°, −15°, 0°, 15°, 30°, 45°) are necessary to analyze the entire scan plane when a precision of $3dB$ is enough. Other solutions are possible, e.g. a step of 20° (5 points) has also validated to be effective. With this configuration the energy required to perform the scan results to be $1.9J$, while with 7 points is $2.7J$, as deduced by (7).

The RAW and SAW energy consumption was compared for equal data rate. Figure 10 reports the energy saving ratio in the form described by eq (13).

$$E_s = 1 - \frac{E_{RAW}(\Delta t)}{E_{SAW}(\Delta t)} \tag{13}$$

$E_s$ is a function of the data transmission duration $\Delta t$ after antenna configuration; the figure is relative to $P_{save} = 18dB$ and $P_{save} = 9dB$. As already discussed, the RAW system obviously starts in energy debit due to the scan phase, with a negative saving factor. In the case of $P_{save} = 18dB$, the breakeven point $E_s = 0$ is obtained at $t_{be} = 9s$ and $t_{be} = 6s$ with a scan of 7 and 5 directions respectively, as from (8). Obviously, with a coarse scan (i.e. less pointing directions) the RAW recover faster. After breakeven, the gain quickly increases with transmit time until saturation to $E_s = 0.28$ (i.e.

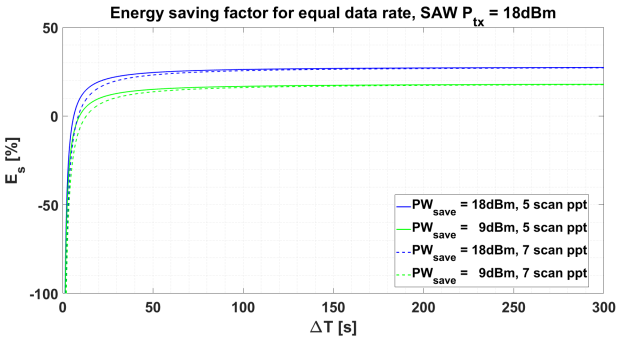


Fig. 10. Power saving factor for equal data rate and breakeven point $t_{be}$.

28% less energy). Instead, a $P_{save} = 9dB$ produces a gain saturation of 19%. In conclusion, the energy gain depends:

- from the power saving $P_{save}$, the larger is this value the greater is the asymptotic energy gain;
- from the scan process, the lower is the time dedicated to this phase the shorter is the time scale the RAW starts to gain.

The breakeven time needs to be accounted to ensure the energy gain of a RAW system especially when the configuration process is required frequently (i.e. dynamic scenario).

### C. Overall energy saving for variable data rate

In this Section, the case where the two systems operate at different data rates is analyzed according to the method presented in Section( II-D). Tables III illustrates all the possible combinations of data rates (RAW vs SAW) and the related energy gain. The energy saving is estimated by using (10) and (9) in (13) for equal transmitted power and a scan process covering 7 directions (i.e. $E_{scan} = 2.7J$, as evaluated in Section( IV-B)). The computation is repeated for different quantities of data to transfer (i.e. $10MB$,$100MB$ and $1GB$). This analysis shows that the RAW system has an energy gain when it transmits faster than the SAW. In this case the consumption is reduced because the RAW system transmits power for less time. In fact, the higher the data rate with respect the standard system, the higher the energy saving. On the contrary, we noticed that when the two systems operate at equal data rate, the RAW toils to recover the scan process (up to reaching a null energy saving for large quantity of data to transfer). Since the data rate is automatically adjusted by the radio module based on the RSSI, in the following we show the energy saving as a function of the distance. In the link budget reported in Figure 11, the receiver sensitivity has been increased by a safety margin of $20dB$ to account for reflections and other sources of interference. For equal transmit power (i.e. $9dBm$), the SAW link achieves maximum rate (i.e. $54Mbps$) for few meters, then significantly drops to the minimum (i.e. $1Mbps$) at around $100m$ to consequently being unable to communicate. On the other hand, the RAW is able to maintain a higher rate along with the SAW operation range. Figure 12 shows the energy saving factor by comparing (9) with (10) for different quantities of transmitted information and in the aforementioned conditions. For a link

TABLE III
POSSIBLE ENERGY SAVING PROVIDED BY THE VARIABLE DATA RATE OPTION

| **RAW Rate** *R[Mbps]* | **SAW Rate** *R[Mbps]* | **@10MB** $E_s[\%]$ | **@100MB** $E_s[\%]$ | **@1GB** $E_s[\%]$ |
|---|---|---|---|---|
| 54 | 54 | -8.5 | -0.9 | -0.1 |
| 54 | 36 | 10.9 | 17.2 | 17.8 |
| 54 | 18 | 42.0 | 46.1 | 46.5 |
| 54 | 11 | 59.7 | 62.6 | 62.9 |
| 54 | 9 | 65.8 | 68.2 | 68.4 |
| 54 | 5 | 77.5 | 79.1 | 79.3 |
| 54 | 2 | 91.2 | 91.8 | 91.7 |
| 54 | 1 | 95.5 | 95.8 | 95.8 |
| 36 | 36 | -7.0 | -0.7 | -0.01 |
| 36 | 18 | 30.4 | 34.5 | 34.9 |
| 36 | 11 | 51.7 | 54.5 | 54.8 |
| 36 | 9 | 58.9 | 61.3 | 61.6 |
| 36 | 5 | 73.0 | 74.6 | 74.8 |
| 36 | 2 | 89.4 | 90.0 | 90.0 |
| 36 | 1 | 94.6 | 94.9 | 94.9 |
| 18 | 18 | -4.6 | -0.5 | -0.1 |
| 18 | 11 | 27.4 | 30.2 | 30.5 |
| 18 | 9 | 38.2 | 40.7 | 40.9 |
| 18 | 5 | 59.5 | 61.0 | 61.2 |
| 18 | 2 | 84.1 | 84.7 | 84.8 |
| 18 | 1 | 91.8 | 92.2 | 92.2 |
| 11 | 11 | -3.2 | -0.3 | 0 |
| 11 | 9 | 12.2 | 14.6 | 14.9 |
| 11 | 5 | 42.4 | 44.0 | 44.1 |
| 11 | 2 | 77.4 | 78.0 | 78.0 |
| 11 | 1 | 88.4 | 88.7 | 88.7 |
| 9 | 9 | -2.7 | -0.3 | 0 |
| 9 | 5 | 32.6 | 34.2 | 34.3 |
| 9 | 2 | 73.5 | 74.1 | 74.2 |
| 9 | 1 | 86.4 | 86.8 | 86.8 |
| 5 | 5 | -1.8 | -0.2 | 0 |
| 5 | 2 | 60.0 | 60.64 | 60.7 |
| 5 | 1 | 79.5 | 79.9 | 79.9 |
| 2 | 2 | -0.71 | -0.1 | 0 |
| 2 | 1 | 48.5 | 48.8 | 48.8 |
| 1 | 1 | -0.4 | 0 | 0 |

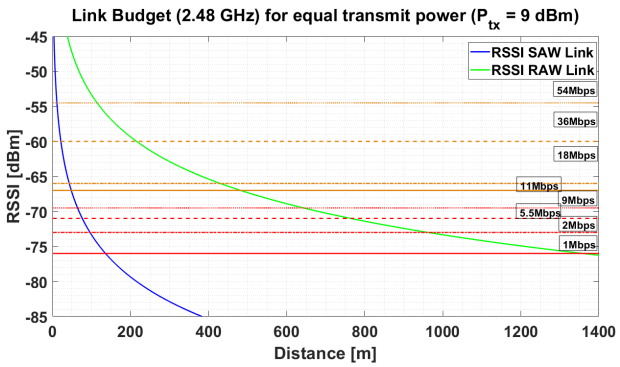


Fig. 11. Link budget computed at $2.48GHz$. Each gap set by the safety margin lines shown the achievable rate. When the RSSI falls in one of the bands, the radio module set a specific data rate.

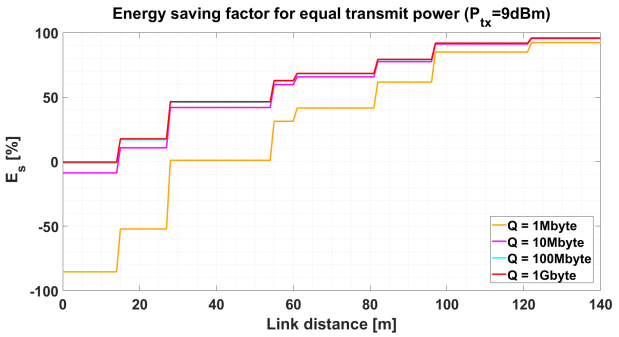


Fig. 12. Energy saving factor for equal transmit power and variable data rate. The saving is shown as a function of link distance $d$ and quantity of transmitted information $Q$; the discontinuities are due changes in data rate along with the distance, according to the link budged analysis in Figure 11.

distance lower than $10m$, there is no benefit in using the RAW system since both wireless links operate at equal rate and transmitted power. In these conditions, and for a small quantity of transmitted data (e.g. $Q = 1MB$) the energy required in the scan phase is not compensated by the ensuing power gain, resulting in a negative energy saving factor. However, even at short distances, the initial overhead is fully recovered for large quantities of transmitted data (i.e. greater than $100MB$), with the energy saving factor approaching zero (i.e. breakeven). Significant saving factors are then obtained at larger distances when the SAW system lower the data rate because of the distance (i.e. received power), while the RAW allows to keep a higher rate. In this case, saving factors that span from 18% to 96% (i.e. $54Mbps$ vs $36Mbps$ and $54Mbps$ vs $1Mbps$ by looking at the curve $Q = 1GB$), can be obtained. Overall, the RAW link achieves best savings on longer distances, especially when the quantity of data to be transmitted is of the order of few $MB$. As for the experimental testing, we first verified power absorption as a function of data rate; this has been done by measuring the absorbed current with different data rates. We observed that power absorption remains unchanged as data rate increases, while absorbed power does drop at times fully coherent with frame duration, in accordance with Tables I and II.

## V. Field Results

### A. In-situ validation of energy saving for equal data rate

The presented system has been installed in the field and the proposed approach validated in real environment. The installation site consists of autonomous IoT-devices placed along motorways. These are composed by the ULP radio platform coupled with a ULP camera board. The latter performs local video processing to detect road traffic events as traffic congestion, wrong way vehicle detection and cycle detection. The result of the local video-processing (i.e. alarm composed by some images and short video on-demand) is transmitted to the edge gateway in real-time. The average distance between nodes and edge gateway is variable between 500-1000$m$, while the edge layer is connected via Ethernet.

The scenario for the tests is reported in Figure 13 and consists in a point-to-point communication between IoT-device and edge gateway placed at a distance of $1km$ along a motorway. Installation of antennas on top of motorway light-poles is difficult (i.e. tricky to direct the antenna radiation towards the desired direction). Autonomous antenna configuration process (i.e. electronic beam steering) is required to enhance the quality of the link and reach the required distance. Figure 14 shows the link budget for the RAW and

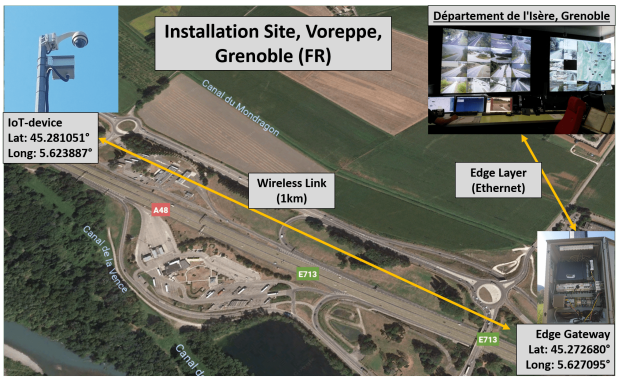


Fig. 13. Google maps snapshot of the installation site in Voreppe, Grenoble, France.

SAW links when transmitting at maximum power ($P_{tx} = 18$ $dBm$). The receiver sensitivity at minimum rate is $-96dBm$ and a safety margin of $20dB$ is added. This means that a safe wireless communication is possible when the RSSI is above the safety margin at the required link-distance. First, we considered the SAW link. From Equation (1), the RSSI at $1km$ link given $-85dBm$ ($11dB$ above the receiver sensitivity). Even at maximum transmit power, the communication link was practically unfeasible. Then, we tested the wireless link with reconfigurable antennas and the same transmit power and link distance ($P_{tx} = 18$ $dBm$, $d = 1$ $km$). Equation (1) given a RSSI of $-65$ $dBm$ ($11dB$ above the safety margin). The gain provided by reconfigurable antennas has been used to reduce the transmit power that also reduced the overall consumption of the node. In a different view, we can said that at parity of transmit power the communication system equipped with reconfigurable antennas can achieve higher link distances (as shown in Figure 14). During on-site experiment, the power

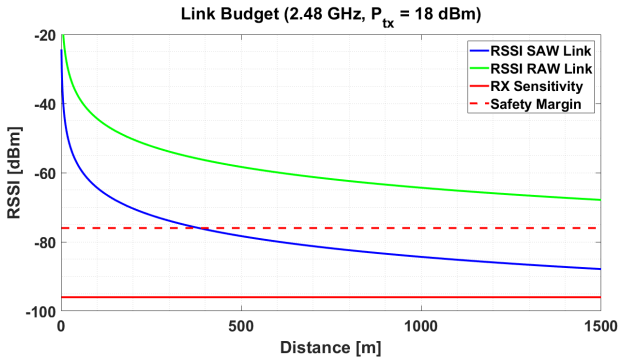


Fig. 14. Link budget estimation at $2.48GHz$ for the RAW and the SAW links at parity of transmit power ($P_{tx} = 18$ $dBm$).

emitted by the transmitter has been reduced to $9dBm$ with respect to the maximum value ($18dBm$), thus providing an

TABLE IV
SENSOR NODE (TX) ANTENNA CONFIGURATIONS - THE CONTENTS REPRESENTS THE ELABORATED RSSI[$dBm$] FOR EACH POINTING DIRECTION OF THE ANTENNA MAIN BEAM.

| **Link directions** $\phi[^\circ]$ | | | | | |
|---|---|---|---|---|---|
| **TEST** | $-40^\circ$ | $-20^\circ$ | $0^\circ$ | $20^\circ$ | $40^\circ$ |
| $Avg.$ | -93 | -92 | -92 | -80 | -78 |

energy saving factor of 19%, as in Figure 10). A significant point is that, improving the antenna gain (e.g. with a 4x4 array) further enhancement in consumption can be achieved. Table IV reports the logs retrieved during the configuration process of the node which demonstrates the capability of the IoT-device antenna to align the beam toward the edge gateway. The best quality of the link is achieved with a scan angle of $40^\circ$ (and more than $15dB$ with respect to the worst value).

### B. In-situ validation of energy saving for variable data rate

During this validation we run into a data rate limitation of the currently employed hardware. We experienced a long latency in between the transmission of consecutive frames, constant with respect to the employed data rate. Performed tests established that the bottleneck is caused by the UART interface between the STM32 Nucleo platform and the IEEE 802.11 b/g SoC radio module. Although this unexpected hardware issue, we replicated the proposed RAW and SAW systems with low-power Banana pi boards [51]. These include an on-board IEEE 802.11 b/g radio in which we integrated the reconfigurable antenna. Then, we verified the behaviour of such radio module by changing the communication distance between the IoT-device and edge gateway, and this test experimentally validated Figure 11. Indeed, the radio module autonomously sets the data rate based on the RSSI level. This confirms the power save factor found in Figure 12, which is valid in spite of the experimentation has replicated with low-power boards. Tests have been performed indoor at $100m$ link distance. We found a RSSI= $-78dBm$ and $-55dBm$ for the SAW and RAW. In these conditions, we measured the time required to transfer $10MB$ of data at the edge gateway side, to evaluated the effective throughput. We found $0.77Mbps$ (i.e. related to $1Mbps$ data rate) and $20Mbps$(related to $36Mbps$ data rate) respectively. According to Figure 14, an energy gain of 95% is obtained for the selected test case.

## VI. CONCLUSIONS AND FUTURE PERSPECTIVES

The paper has addressed the implementation of reconfigurable antennas on SoC radios demonstrating its feasibility on new generation ULP radio platforms. Our research has demonstrated that reconfigurable antennas reduce the overall energy consumption of the wireless link, and provide a more efficient communication. The effectiveness of the system has been validated and tested in the field. We found that the design of the antenna gain and the beamforming capability plays an important role in the consumption as well as the performance of the overall WSN(s) subsystem. Such antenna design should maximize the date rate while keeping the transmit power of the radio at the minimum value, which also reduce signal distortions. A combination of these achieves the greatest advantage in energy saving. We have verified that further enhancement are presently hindered by current ULP hardware limitations, with good prospect for future systems. Work is currently underway to address a limitation of the present beam-steering; with a standard steerable beam antenna the edge gateway can only direct its beam toward the direction of one sensor node at a time. An improved version of this work will show a novel multi-beams antenna array concept which is currently under investigation to remove this limitation. Furthermore, the emergent availability of new high-throughput wireless standards (i.e., IEEE 802.11 ay) will be a valuable option to extends this work at the edge layer which currently use ethernet connection.

## ACKNOWLEDGMENT

This work was supported by the OPERA project, which has received funding from the European Union H2020 call ICT4-2015 programme under grant agreement No. 688386.

## REFERENCES

[1] M. T. Lazarescu, "Design of a WSN Platform for Long-Term Environmental Monitoring for IoT Applications," *IEEE Journal on Emerging and Selected Topics in Circuits and Systems*, vol. 3, no. 1, pp. 45 – 54, Mar. 2013, doi:10.1109/JETCAS.2013.2243032.

[2] S. Bera, S. Misra, S. K. Roy, and M. S. Obaidat, "Soft-WSN: Software-Defined WSN Management System for IoT Applications," *IEEE Systems Journal*, vol. 12, no. 3, pp. 2074 – 2081, Mar. 2018, doi:10.1109/JSYST.2016.2615761.

[3] A. Čolaković and M. Hadžialić, "Internet of Things (IoT): A review of enabling technologies, challenges, and open research issues," *Computer Networks*, vol. 144, pp. 17 – 39, Oct. 2018, doi:10.1016/j.comnet.2018.07.017.

[4] R. Fantacci, T. Pecorella, R. Viti, and C. Carlini, "A network architecture solution for efficient IOT WSN backhauling: challenges and opportunities," *IEEE Wireless Communications*, vol. 21, no. 4, pp. 113 – 119, Aug. 2014, doi:10.1109/MWC.2014.6882303.

[5] L. Davoli, L. Belli, A. Cilfone, and G. Ferrari, "From Micro to Macro IoT: Challenges and Solutions in the Integration of IEEE 802.15.4/802.11 and Sub-GHz Technologies," *IEEE Internet of Things Journal*, vol. 5, no. 2, pp. 784 – 793, Apr. 2018, doi:10.1109/JIOT.2017.2747900.

[6] A. Zanella, N. Bui, A. Castellani, L. Vangelista, and M. Zorzi, "Internet of Things for Smart Cities," *IEEE Internet of Things Journal*, vol. 1, no. 1, pp. 22 – 32, Feb. 2018, doi:10.1109/JIOT.2014.2306328.

[7] F. Zhang, M. Liu, Z. Zhou, and W. Shen, "An IoT-Based Online Monitoring System for Continuous Steel Casting," *IEEE Internet of Things Journal*, vol. 3, no. 6, pp. 1355 – 1363, Aug. 2016, doi:10.1109/JIOT.2016.2600630.

[8] L. Chen, N. Zhao, Y. Chen, F. R. Yu, and G. Wei, "Over-the-air Computation for IoT Networks: Computing Multiple Functions with Antenna Arrays," *IEEE Internet of Things Journal ( Early Access )*, pp. 1 – 12, Jun. 2018, doi:10.1109/JIOT.2018.2843321.

[9] W. Na, Y. Lee, N.-N. Dao, D.-N. Vu, A. Masood, and S. Cho, "Directional Link Scheduling for Real-time Data Processing in Smart Manufacturing System," *IEEE Internet of Things Journal ( Early Access )*, pp. 1 – 10, Aug. 2018, doi:10.1109/JIOT.2018.2865756.

[10] J. P. M. Torregoza, I.-Y. Kong, and W.-J. Hwang, "Wireless Sensor Network Renewable Energy Source Life Estimation," in *Proc. of the First International Conference on Communications and Electronics, Hanoi, Vietnam*, Oct. 2006, pp. 373 – 378, doi:10.1109/CCE.2006.350799.

[11] L. Pilosu, L. Mossucca, A. Scionti, G. Giordanengo, F. Renga, P. Ruiu, O. Terzo, S. Ciccia, and G. Vecchi, "An Energy Efficient Communication Protocol for Low Power, Energy Harvesting Sensor Modules," *In: Xhafa F., Barolli L., Amato F. (eds) Advances on P2P, Parallel, Grid, Cloud and Internet Computing. 3PGCIC. Lecture Notes on Data Engineering and Communications Technologies*, vol. 1, pp. 221 – 232, Oct. 2016, doi:10.1007/978-3-319-49109-7_21.

[12] G. Giordanengo, L. Pilosu, L. Mossucca, F. Renga, S. Ciccia, O. Terzo, G. Vecchi, V. Romano, and I. Hunstad, "Energy Efficient System for Environment Observation," in *Proc. of the Int. Conf. on Complex, Intelligent, and Software Intensive Systems (CISIS), Torino, Italy*, July 2017, pp. 987 – 999, doi:10.1007/978-3-319-61566-0-93.

[13] H. Sharma, A. Haque, and Z. A. Jaffery, "Solar energy harvesting wireless sensor network nodes: A survey," *Journal of Renewable and Sustainable Energy*, vol. 10, no. 2, Feb. 2018, doi:10.1063/1.5006619.

[14] C. S. Abella, S. Bonina, A. Cucuccio, S. DAngelo, G. Giustolisi, A. D. Grasso, A. Imbruglia, G. S. Mauro, G. A. Nastasi, G. Palumbo, S. Pennisi, G. Sorbello, and A. Scuderi, "Autonomous Energy-Efficient Wireless Sensor Network Platform for Home/Office Automation," *IEEE Sensors Journal ( Early Access )*, pp. 1 – 1, Gen. 2019, doi:10.1109/JSEN.2019.2892604.

[15] D. Basu, G. S. Gupta, G. Moretti, and X. Gui, "Energy Efficiency Comparison of a State Based Adaptive Transmission Protocol with Fixed Power Transmission for Mobile Wireless Sensors," *Journal of Telecommunications System and Management*, vol. 6, no. 1, 2017, doi:10.4172/2167-0919.1000149.

[16] Z. Zhou, J. Xu, Z. Zhang, F. Lei, and W. Fang, "Energy-Efficient Optimization for Concurrent Compositions of WSN Services," *IEEE Access*, vol. PP, no. 99, pp. 657 – 660, Sept. 2017, doi:10.1109/ACCESS.2017.2752756.

[17] D. Purkovic, M. Hönsch, and T. R. M. K. Meyer, "An Energy Efficient Communication Protocol for Low Power, Energy Harvesting Sensor Modules," *IEEE Sensors Journal*, vol. 19, no. 2, pp. 701 – 714, Jan. 2019, doi:10.1109/JSEN.2018.2876746.

[18] C. Tantur, H. U. Yildiz, S. Kurt, and B. Tavli, "Optimal transmission power level sets for lifetime maximization in wireless sensor networks," in *Proc. of the IEEE SENSORS, Orlando, FL, USA*, Nov. 2017, pp. 1 – 3, doi:10.1109/ICSENS.2016.7808888.

[19] P. Le-Huy and S. Roy, "Low-Power 2.4 GHz Wake-Up Radio for Wireless Sensor Networks," in *Proc. of the IEEE Int. Conf. on Wireless and Mobile Computing, Networking and Communications, Avignon, France*, Oct. 2008, pp. 13 – 18, doi:10.1109/WiMob.2008.54.

[20] G. Manes, R. Fantacci, F. Chiti, M. Ciabatti, G. Collodi, D. D. Palma, I. Nelli, and A. Manes, "Energy efficient MAC protocols for Wireless Sensor Networks endowed with directive antennas: a cross-layer solution," in *Proc. of the IEEE Radio and Wireless Symposium, Orlando, FL, USA*, Mar. 2008, pp. 239 – 242, doi:10.1109/RWS.2008.4463473.

[21] G. Dassano and M. Orefice, "Voltage Controlled Steerable Array for Wireless Sensors Networks," in *Proc. of the Eur. Conf. on Antennas and Propagation (EuCAP), Edinburgh, UK*, Feb. 2007, pp. 1 – 4, doi:10.1049/ic.2007.1269.

[22] M. Hanaoui and M. Rifi, "Directional communications with smart antenna system to improve energy efficiency in wireless sensor networks," in *Proc. of the Int. Conf. on Electrical and Information Technologies (ICEIT), Tangiers, Morocco*, May 2016, pp. 203 – 207, doi:10.1109/EITech.2016.7519590.

[23] B. Gerislioglu, A. Ahmadivand, M. Karabiyik, R. Sinha, and N. Pala, "Vo2based reconfigurable antenna platform with addressable microheater matrix," *Advanced Electronic Materials*, vol. 3, pp. 1 – 8, Jun. 2017, doi:10.1002/aelm.201700170.

[24] M. Mofolo and A. A. Lysko, "Incorporating antenna beamswitching technique into drivers for IEEE 802.11 WLAN devices," in *Proc. of the IEEE Int. Conf. on Communications (MICC), Kuching, Sarawak, Malaysia*. IEEE Conference Publications, Oct 2015, pp. 96 – 101, doi:10.1109/MICC.2015.7725415.

[25] L. Catarinucci, S. Guglielmi, R. Colella, and L. Tarricone, "Pattern-Reconfigurable Antennas and Smart Wake-Up Circuits to Decrease Power Consumption in WSN Nodes," *IEEE Sensors Journal*, vol. 14, no. 12, pp. 4323 – 4324, 2014, doi:10.1109/JSEN.2014.2360939.

[26] T. N. Le, A. Pegatoquet, T. L. Huy, L. Lizzi, and F. Ferrero, "Improving Energy Efficiency of Mobile WSN Using ReconfigurableDirectional Antennas," *IEEE Communications Letters*, vol. 20, no. 6, pp. 1243 – 1246, 2016, doi:10.1109/LCOMM.2016.2554544.

[27] A. A. Lysko, "Towards an ultra-low-power electronically controllable array antenna for WSN," in *Proc. of the IEEE-APS Topical Conf. on Antennas and Propagation in Wireless Communications (APWC), Cape Town, South Africa*, Oct 2012, pp. 642 – 645, doi:10.1109/APWC.2012.6324932.

[28] E. D. Skiani, S. A. Mitilineos, and S. C. A. Thomopoulos, "A Study of the Performance of Wireless Sensor Networks Operating with Smart Antennas," *IEEE Antennas and Propagation Magazine*, vol. 54, no. 3, pp. 50 – 67, Aug. 2012, doi:10.1109/MAP.2012.6293950.

[29] R. R. Rout, S. Ghosh, and S. K. Ghosh, "Efficient data collection with directional antenna and network coding in wireless sensor networks," in *Proc. of the Conf. on Advanced Networks and Telecommuncations Systems (ANTS), Bangalore, India*, June 2013, pp. 81 – 86, doi:10.1109/ANTS.2012.6524233.

[30] K. Kucuk, A. Kavak, and H. Yigit, "A Smart Antenna Module Using OMNeT++ for Wireless Sensor Network Simulation," in *Proc. of the Int. Symp. on Wireless Communication Systems (ISWCS), Trondheim, Norway*, Dec. 2007, pp. 747 – 751, doi:10.1109/ISWCS.2007.4392440.

[31] R. M. Sandoval, A.-J. Garcia-Sanchez, J. Garcia-Haro, and T. M. Chen, "Optimal Policy Derivation for Transmission Duty-Cycle Constrained LPWAN," *IEEE Internet of Things Journal*, vol. 5, no. 4, pp. 3114 – 3125, Aug. 2018, doi:10.1109/JIOT.2018.2833289.

[32] I. Tomi and J. A. McCann, "A Survey of Potential Security Issues in Existing Wireless Sensor Network Protocols," *IEEE Internet of Things Journal*, vol. 4, no. 6, pp. 1910 – 1923, Sept. 2017, doi:10.1109/JIOT.2017.2749883.

[33] M. Frustaci, P. Pace, G. Aloi, and G. Fortino, "Evaluating Critical Security Issue of the IoT World: Present and Future Challenges," *IEEE Internet of Things Journal*, vol. 5, no. 4, pp. 2483 – 2495, Aug. 2018, doi:10.1109/JIOT.2017.2767291.

[34] E. Cianca, M. D. Sanctis, and S. D. Domenico, "Radios as Sensors," *IEEE Internet of Things Journal*, vol. 4, no. 2, pp. 363 – 373, Apr. 2017, doi:10.1109/JIOT.2016.2563399.

[35] M. R. Palattella, M. Dohler, A. Grieco, G. Rizzo, J. Torsner, T. Engel, and L. Ladid, "Internet of Things in the 5G Era: Enablers, Architecture, and Business Models," *IEEE Journal on Selected Areas in Communications*, vol. 34, no. 3, pp. 510 – 527, Feb. 2016, doi:10.1109/JSAC.2016.2525418.

[36] M. Jusoh, T. Sabapathy, M. F. Jamlos, and M. R. Kamarudin, "Reconfigurable four-parasitic-elements patch antenna for high-gain beam switching application," *IEEE Antennas and Wireless Propagation Letters*, vol. 13, pp. 79 – 82, Jan. 2014, doi:10.1109/LAWP.2013.2296491.

[37] L. Lizzi, F. Ferrero, J. M. Ribero, R. Staraj, T. N. Le, A. Pegatoquet, and L. H. Trinh, "Differential pattern-reconfigurable antenna prototype for efficient wireless sensor networks," in *Proc. of the IEEE Int. Symp. on Antennas and Propagation (APSURSI), Fajardo, Puerto Rico*, Oct. 2016, pp. 1239 – 1240, doi:10.1109/APS.2016.7696327.

[38] M. Rzymowski, P. Woznica, and L. Kulas, "Single-Anchor Indoor Localization Using ESPAR Antenna," *IEEE Antennas and Wireless Propagation Letters*, vol. 15, pp. 1183 – 1186, Nov. 2015, doi:10.1109/LAWP.2015.2498950.

[39] A. Dihissou, A. Diallo, P. L. Thuc, and R. Staraj, "Technique to increase directivity of a reconfigurable array antenna for wireless sensor network," in *Proc. of the Eur. Conf. on Antennas and Propagation (EUCAP), Paris, France, France*, May 2017, pp. 606 – 610, doi:10.23919/EuCAP.2017.7928636.

[40] Antenova, "Antenova m2m, 2.4 GHz Antennas," last access on Sept. 20, 2018. [Online]. Available: http://www.antenova-m2m.com/product/2-4-ghz-rufa-right-smd-antennas/#

[41] F. Gross, "Chapter 3: Antenna Fundamentals," in *Smart Antennas for Wireless Communications with Matlab (McGraw-Hill Companies)*, 2005, doi:10.1036/007144789X.

[42] STM, "SPWF01SC Serial-to-Wi-Fi b/g/n intelligent modules," last access on Feb. 08, 2019. [Online]. Available: http://www.st.com/resource/en/datasheet/spwf01sc.pdf

[43] ——, "STM32L476XX Ultra-low-power ARM Cortex-M4 32-bit MCU+FPU," last access on Feb. 07, 2019. [Online]. Available: https://www.st.com/resource/en/datasheet/stm32l476rg.pdf

[44] T. A. Milligam, "Chapter 6: Aperture-coupled Stacked Patches," in *Modern Antenna Design, 2nd ed (John Wiley and Sons)*, July 2005, isbn:978-0-471-45776-3.

[45] ISOLA, "IS400 High Performance Laminate and Prepreg," last access on Feb. 09, 2019. [Online]. Available: https://www.eurocircuits.de/wp-content/uploads/Document/IS400-High-Performance-Laminate-and-Prepreg-Isola.pdf

[46] ENVONIK, "Rohacell HF31 - Negligible Absorption in the High Frequency Range," last access on Feb. 09, 2019. [Online]. Available: https://www.rohacell.com/product/peek-industrial/downloads/rohacell%20hf%20product%20information.pdf

[47] C. A. Balanis, "6.3 N-Element Linear Array: Uniform Amplitude and Spacing," in *Antenna Theory - Analysis and Design, 3rd ed (John Wiley and Sons)*, 2005, isbn:0-471-66782-X.

[48] E. C. Niehenke, V. V. DiMarco, and A. Friedberg, "Linear Analog Hyperabrupt Varactor Diode Phase Shifters," in *Proc. of the IEEE Int. Microwave Symposium Digest (MTT-S), St. Louis, MO, USA, USA*, Feb. 1985, pp. 657 – 660, doi:10.1109/MWSYM.1985.1132067.

[49] SKYWORKS, "SMVA1248-079LF: Hyperabrupt Junction Tuning Varactor," last access on Feb. 09, 2019. [Online]. Available: http://www.skyworksinc.com/uploads/documents/SMVA1248_079LF_203203C.pdf

[50] MICROCHIP, "MCP6001/1R/1U/2/4: 1 MHz, Low-Power Op Amp," last access on Feb. 18, 2019. [Online]. Available: https://ww1.microchip.com/downloads/en/DeviceDoc/21733j.pdf

[51] BPI, "BPI Home, Banana Pi Single Board Computers," last access on Oct. 29, 2018. [Online]. Available: http://www.banana-pi.org/